Measuring Grain Junction Angles in Discretized Microstructures

MICHAEL CHANDROSS and ELIZABETH A. HOLM

Grain junction angles control microstructural morphology and evolution, but because they are difficult to measure, they are reported rarely. We have developed a method, based on the optimization of the Pearson's correlation coefficient, to measure grain junction angles in planar discretized microstructures without converting or remeshing the original data. We find that the grain junction angle distribution of equiaxed, relatively isotropic, three-dimensional (3D) microstructures is a Gaussian distribution centered about 120 deg, with a larger width than predicted primarily because of boundary energy anisotropy. Short boundary segments, which occur primarily in sections of 3D microstructures, cause anomalous peaks in the grain junction angle distribution that provide a marker for sample dimensionality. The grain junction angle distribution is a characterization metric for digitized microstructures, revealing the effects of grain boundary energy anisotropy, simulation parameters, and dimensionality.

DOI: 10.1007/s11661-010-0355-7

I. INTRODUCTION

As Smith[1] noted 60 years ago, the angles at grain triple junctions control not only grain shape and microstructural morphology but also grain growth itself. The triple-junction angle results from the balance of surface tensions at the line where the boundary sheets meet according to the Herring relation.[2] For isotropic grain boundary free energy, all grain junction lines will be triple junctions, and all angles will be equal and 120 deg. When boundary energies vary, triple-junction angles will deviate from 120 deg, and other line junctions, such as quad junctions, may become stable. These deviations may have significant effects on microstructural evolution. For instance, Smith noted in 1952 that "…grain growth will slow and stop (in the absence of inclusions) only when grain corner angles can depart from 120 degrees…"[1]

Grain junctions are linear objects in three-dimensional (3D) space. However, microstructures typically are analyzed in two-dimensional (2D) cross sections. Because the probability of sectioning each grain junction orthogonally is vanishingly small, there is a distribution of observed grain junction angles, even in an isotropic polycrystal. Harker and Parker[3] derived the observed triple-junction angle distribution for an isotropic microstructure in 1945. As they recognized, a deviation from that distribution indicates either that triple junctions deviate from 120 deg or that the triple lines are not distributed randomly (*e.g.*, in a columnar structure where most triple lines are parallel to each other).

MICHAEL CHANDROSS, Principal Member of Technical Staff, and ELIZABETH A. HOLM, Distinguished Member of Technical Staff, are with the Department of Computational Materials Science and Engineering, Sandia National Laboratories, Albuquerque, NM 87185-1411. Contact e-mail: eaholm@sandia.gov

Manuscript submitted April 6, 2010.
Article published online July 27, 2010

Because of its important relationships to boundary energy and microstructural evolution, the triple-junction angle distribution has been measured for a variety of single-phase and multiphase alloys (*cf.* References 3 through 12). Because of the difficulty of obtaining 3D representations of a microstructure, early studies of triple-junction angles typically were restricted to manual measurement of triple junctions in an optical micrograph of a planar cross section.[3,7,10,11] Because data sets were tedious to obtain and were limited in statistics, the triple-junction angle distribution was not used widely in microstructural characterization. With the advent of more efficient serial sectioning and data reconstruction techniques, the focus shifted to measuring 2D[12] or true, 3D triple-junction angles[4–6,8,9] using automated methods to determine grain boundary properties. Although the new methods permit much higher throughput, they are still specialized, and triple-junction angles are not yet used routinely to characterize microstructures.

Recent systems of microstructural representation present a new complication. Although traditional micrographs were recorded on analog film, some current techniques describe microstructures digitally. Of particular interest in this work are representations in which grains are bitmapped so that each volume element of a grain is represented by a pixel (2D) or a voxel (3D); two examples are shown in Figure 1.[13] In this case, grain boundaries are implicit; they occur where unlike pixels/voxels meet. Furthermore, because the volume elements are placed regularly, grain boundaries conform to the pixel/voxel lattice and may be rough. This type of microstructural representation is common in computer simulation (especially Monte Carlo Potts model [MCPM], cellular automaton, and some phase field models) and in experiments (particularly electron backscatter diffraction microscopy [EBSD] but also some digital image analysis packages).

As will be discussed, measuring grain junction angles in such microstructures is problematic primarily because

the tangent to the boundary at the grain junction is not defined uniquely, so there is no definition of the "correct" junction angle. Other studies circumvent this problem by preconditioning the data using optical image analysis algorithms that convert the grain boundaries into continuous curves[5,6] by remapping the grain structure to a digitized grain boundary network representation[12] or by remeshing the digitized grain boundaries via triangulation.[4,8,9] In this article, we present a robust and efficient method to measure grain junction angles in planar discretized microstructures without converting or remeshing the original data. This method is applicable to experimental and simulated structures. We find that the resulting grain junction angle distributions can help characterize microstructures in several useful ways.

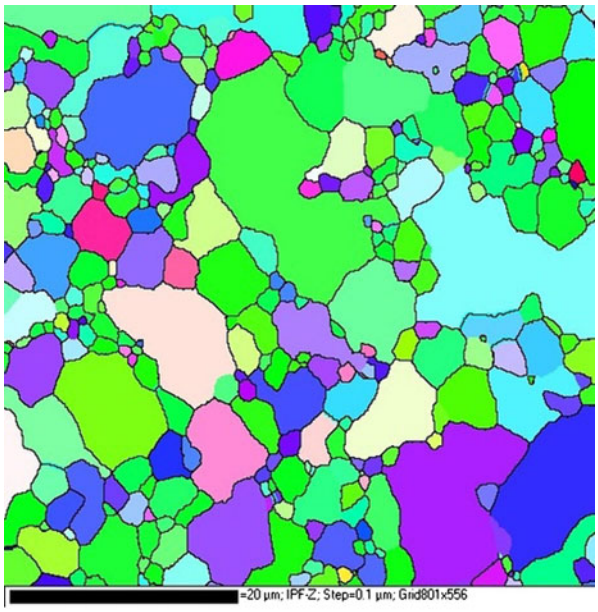

(a)

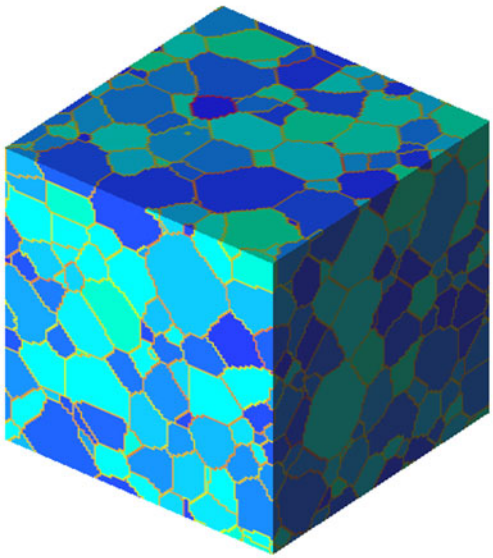

(b)

Fig. 1—Examples of discretized microstructures. (*a*) EBSD image of a columnar polycrystalline Al specimen. Microstructure is bitmapped onto a 2D lattice of pixels.[13] Scale bar is 20 μm. (*b*) Polycrystalline microstructure simulated by an MCPM grain growth simulation. Microstructure is bitmapped onto a 3D lattice of voxels.

II. METHOD

Nearly all experimental micrographs are 2D slices or surfaces; therefore, we restrict ourselves to examining grain junction angles in 2D sections. However, we can use this technique to analyze 3D microstructures by examining various cross sections.

The desired result of this calculation is to achieve angles between tangents to grain boundaries at grain junctions in discretized microstructures where grains are bitmapped onto a regular lattice of voxels, and the color or index of the voxel corresponds to its grain membership. Because grains and grain boundaries are discretized, the tangents are poorly defined. An example of a discrete triple junction is shown in Figure 2. As an extreme example, consider the case in which the grain boundaries are considered only to extend one voxel away from the triple junction. The junction angle θ calculated in this case would be 180 deg. Even for the simple example shown in Figure 2, this is clearly not a good representation of the true triple-junction angle.

A more accurate method to determine an approximate tangent to a discretized grain boundary involves calculating some kind of linear fit to the boundary, as suggested in Reference 12. To arrive at such a fit, it is necessary first to acquire a representation of the boundary. This information is present only implicitly in a discretized microstructure because the voxels themselves only contain information about grain membership and not about the presence of interfaces. To determine grain boundaries, the voxels themselves are much less important than the sites that make up the dual of the lattice. Although previous studies have

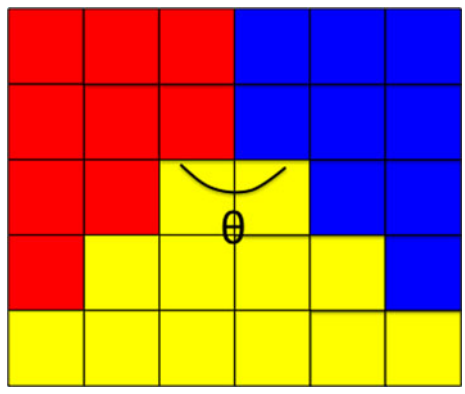

Fig. 2—An example of a discretized 2D triple junction with dihedral angle θ. Grain membership is indicated by voxel color, and grain boundaries are line segments that separate voxels of unlike color.

discretized the grain boundaries on the dual lattice so that a boundary is a body made up of grain boundary pixels/voxels,[12] we choose to treat the boundary site as an object that represents a line segment (in 2D) or a planar facet (in 3D). This approach retains the correct dimensionality for the grain boundaries and avoids the ambiguities that develop when boundaries have finite widths. In the following discussion, we will assume that all calculations are being performed on cubic lattices, implying that any given site has four nearest neighbor voxels in a plane. We classify boundary sites according to the number of unlike neighbor grains. If a site's neighbor voxels are identical, then it is in the interior of a grain (type 1) and is not of interest to us here. A boundary site with two unlike neighbor voxels will be a grain boundary (type 2), except in the special case shown in Figure 3. In this case, we will consider the boundary site to be a quad junction (type 4) to account for the possibility that this represents two grains that either are merging or are splitting. Boundary sites that have three or four distinct grains among their neighbor voxels are triple (type 3) or quad (type 4) junctions, respectively.

The procedure to map out a grain boundary proceeds as follows. First, all boundary sites are identified as one of the types previously defined. The code then moves to the first triple/quad point to begin determining angles. For a given pair of grains, the boundary is followed (*i.e.*, by moving to the next boundary site of type 2 bounded by the appropriate neighbor voxels and keeping track of the direction of movement) until a terminal triple/quad point is reached. This process maps out a discrete grain boundary in space; an example of a discrete grain boundary is shown in Figure 4.

With an accurate spatial representation of the grain boundary, we are now in a position to determine a best linear fit. Fits are calculated with a linear regression algorithm with one restriction—namely that the intercept is forced to be at $x = y = 0$ (*i.e.*, at the triple/quad point) so that all grain boundaries will intersect at a single point. Recall that the correlation coefficient χ^2 for a linear fit of the form $y = ax$ to a series of points (x_i, y_i) is defined as follows:

$$\chi^2 = \sum_{i=1}^{n} (y_i - ax_i)^2 \quad [1]$$

where n is the number of points fit and a is the slope of the line (*i.e.*, $a = \tan^{-1}\theta$, where θ is the angle of the line with respect to the x-axis). Minimizing χ^2 with respect to a and solving for a gives the following:

$$a = \frac{\sum_{i=1}^{n} x_i y_i}{\sum_{i=1}^{n} x_i^2} \quad [2]$$

Examples of linear fits to n boundary points are shown by the blue lines in Figure 4. Note that this formulation precludes θ values greater than 180 deg. Although grain junctions greater than 180 deg are not permitted by the Herring relation, if they do occur in our microstructures, then we report the conjugate angle (360 deg – θ).

For a boundary containing n sites (*i.e.*, consisting of n discrete segments), there are n possible linear fits to the boundary. Previous studies simply have selected an arbitrary number of points for the fit,[12] but the resulting line may be a poor representation of the boundary tangent if n is too low or too high, as shown in Figure 4. Because the linear regression algorithm relies on minimizing χ^2, this parameter is not useful to determine which of the n possible linear fits is the most accurate. Instead, we calculate Pearson's correlation coefficient r[14] for the various fits to use as the relevant parameter. This coefficient is calculated by dividing the covariance of two variables cov(x,y) by the product of their standard deviations σ_x and σ_y. For a series of points (x_i, y_i), r is expressed as follows:

$$r = \frac{\mathrm{cov(x,y)}}{\sigma_x \sigma_y} = \frac{\sum_{i=1}^{n} (x_i - \bar{x})(y_i - \bar{y})}{\sqrt{\sum_{i=1}^{n} (x_i - \bar{x})^2} \sqrt{\sum_{i=1}^{n} (y_i - \bar{y})^2}} \quad [3]$$

where $\bar{x}$ is the mean x value and $\bar{y}$ is the mean y value. Pearson's correlation coefficient determines the amount

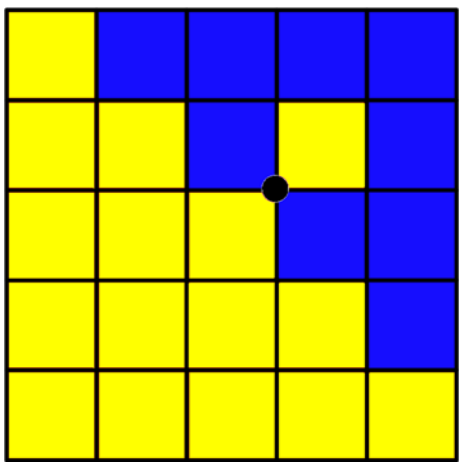

Fig. 3—The site indicated by the black dot is a boundary site with two unlike neighbor grain types that represents a grain junction as opposed to a grain boundary.

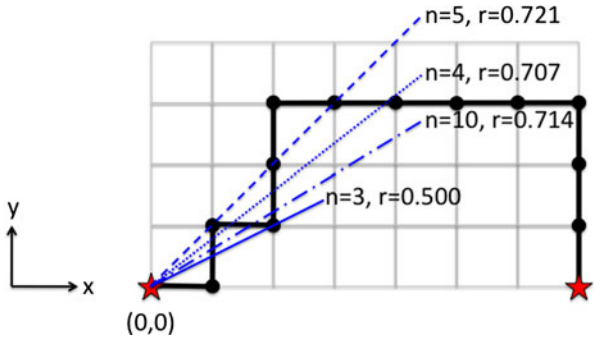

Fig. 4—A discretized boundary resulting from the procedure described in the text. Triple/quad points are denoted by red stars, the boundary sites are black dots, the underlying lattice of voxels is outlined in gray, and the grain boundary is shown as a heavy black line. Also shown are linear fits, computed using Eq. [2], to $n = 3$ (solid blue line), $n = 4$ (dotted blue line), $n = 5$ (dashed blue line), and $n = 10$ (dot-dashed blue line) sites as well as the Pearson's correlation coefficient r for each fit.

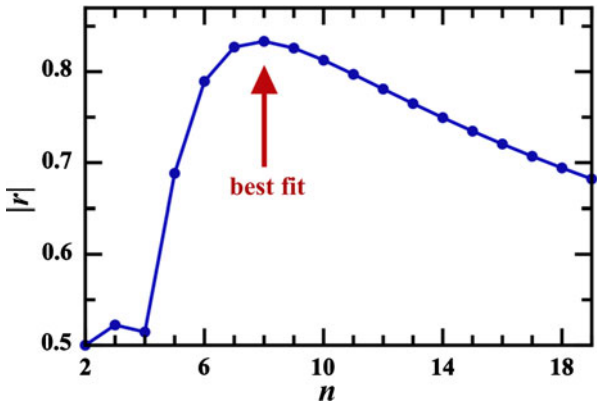

Fig. 5—Pearson's correlation coefficient $|r|$ as a function of the number of grain boundary segments in the fit n for a representative grain boundary in the microstructures studied here. The best fit, determined by the maximum value of $|r|$ before the steady decrease, is indicated by the red arrow.

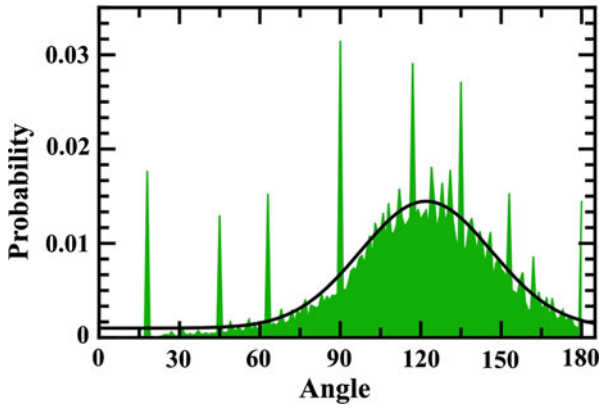

Fig. 6—A representative distribution of grain junction angles for a 3D-simulated polycrystal using the method described in the text. The solid black line shows a fit to a Gaussian distribution with a mean of about 120 deg.

of correlation between two variables. In this case, $|r|$ determines how reasonable a linear fit is to the given segment. As the length increases from 1 to n for a given boundary, $|r|$ starts at 1.0 (because a linear fit to a segment of length 1 is, by definition, exact) and then often drops to low values for extremely short segments. As the boundary length increases, $|r|$ increases rapidly, remains high, and then decreases steadily as the boundary starts to curve. The best linear fit is the largest value of $|r|$ before the decrease. Figure 4 shows these trends in the four fits pictured, and Figure 5 gives a complete plot of $|r|$ *vs* n for a representative boundary in the microstructures studied here with the best fit indicated.

This fitting procedure is repeated for all three or four grain boundaries at a given triple or quad point, respectively, to determine the best fits to all tangents. Angles between these tangents now can be calculated easily, and the procedure is repeated for all triple and quad junctions in the 2D slice. For accurate statistics in a 3D microstructure, these results can be averaged across slices in all three dimensions as discussed subsequently.

III. RESULTS AND DISCUSSION

A. *Grain Junction Angle Distribution*

An example of the distribution of grain junction angles arrived at by this method is shown in Figure 6. The microstructure in this figure is generated by a 3D MCPM simulation of pure, single-phase grain growth,[15,16] The system was a 150 × 150 × 150 voxel cubic lattice evolved from an initially random structure under appropriate conditions to approximate isotropic grain growth (simulation temperature $T = 1.5$, cubic lattice with first-, second-, and third-neighbor interactions); the microstructure seems similar to that shown in Figure 1(b). After evolution for 100 timesteps, we calculated the average grain radius R. The grain junction angle calculation then was performed for a series of 2D slices of the microstructure separated by R to improve statistics without introducing artificial correlations by analyzing slices that are close to each other. By using this method to average across statistically distinct slices in the microstructure in all three directions, we can arrive at improved statistics for histograms such as those in Figure 6 while still simulating relatively small systems.

Several interesting features are evident in the angular distribution. The distribution is approximately Gaussian and peaked near 120 deg, as expected for a perfectly regular distribution of triple-junction angles in a plane. The distribution also shows sharp peaks at 18 deg, 45 deg, 63 deg, 90 deg, 117 deg, 135 deg, 153 deg, 162 deg, and 180 deg. Most of these peaks can be attributed to fits to short boundaries as discussed subsequently.

B. *Effects of Short Boundary Segments*

Short segments are unavoidable in a discretized microstructure. Some grains are naturally small because they are in the process of shrinking and disappearing. Two-dimensional slices of 3D microstructures contain proportionately more small grains because all cross sections of a 3D equiaxed grain (except for one) are smaller than the nominal grain radius. Finally, both simulated and experimental microstructures evince single-site grains along rough grain boundaries, as shown in Figure 3. All these small grains are bounded by short, discretized boundaries.

The number of curve fits that a boundary can be tested against is no more than the number of boundary segments n. The limited number of fits means that only a limited number of tangent angles can be measured for short boundaries. Furthermore, as shown in Figure 5, fits for small n tend to be of poor quality. Figure 7 illustrates the catalog of grain boundaries and best-fit tangents for boundaries of length 1 and 2 segments. Both the limited number of allowable angles and the poor quality fits are apparent.

A notable asymmetry is found in the tangent angle calculation in Figure 7. Recall that the linear fits used to calculate tangent angles are required both to minimize

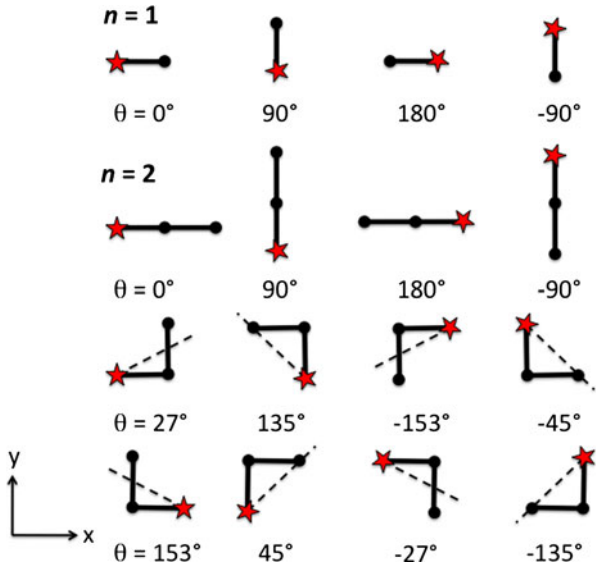

Fig. 7—Catalog of boundary segments of lengths $n = 1$ and $n = 2$. The grain junction is shown by a star; heavy solid lines are boundary segments, and dots indicate boundary sites used for the linear fit, which is shown by a dashed line. (Note that for linear boundary segments, the fit is coincident with the boundary.) θ is the angle between the linear fit for the boundary and the x-axis.

χ^2 and to pass through the origin. This formalism discounts points with x-coordinates of zero, weighting the curve fit toward points with finite x-coordinates, as shown in Eq. [2]. The effect of this asymmetry is minimal for long (large n) boundaries because $x = 0$ points are relatively infrequent. However, for short boundaries, such points may skew the fit substantially.

In equiaxed microstructures, the boundaries of a given grain tend to be of similar lengths. Therefore, the grain junctions in small grains tend to comprise two short boundaries. If we combine all short boundary segments shown in Figure 7 into pairs, then we find that the included grain junction angles are limited to 18 deg, 45 deg, 63 deg, 72 deg, 90 deg, 108 deg, 117 deg, 135 deg, 153 deg, 162 deg and 180 deg. With the exception of 72 deg and 108 deg (which do not seem peaked), these are precisely the grain junction angles that show anomalous peaks in Figure 6. Note that the peaks at 18 deg and 162 deg are a result of the grain configuration shown in Figure 3.

If the anomalous peaks in the distribution are caused by short grain boundaries, then we can eliminate these peaks by including only longer boundaries in our calculation. In Figures 8(a) through (c), we show the same data as in Figure 6 but with the restriction that the minimum boundary length must be two, three, or four segments, respectively.

By enforcing a restriction to segments with a minimum length of two (i.e., no single-segment boundaries), we see a decrease in all anomalous peaks except 18 deg and 162 deg, with the greatest decreases at 45 deg, 63 deg, and 180 deg. Because the peaks at 18 deg and 162 deg are a result of a grain configuration that contains no single segment boundaries, we do not expect these peaks to disappear in this case.

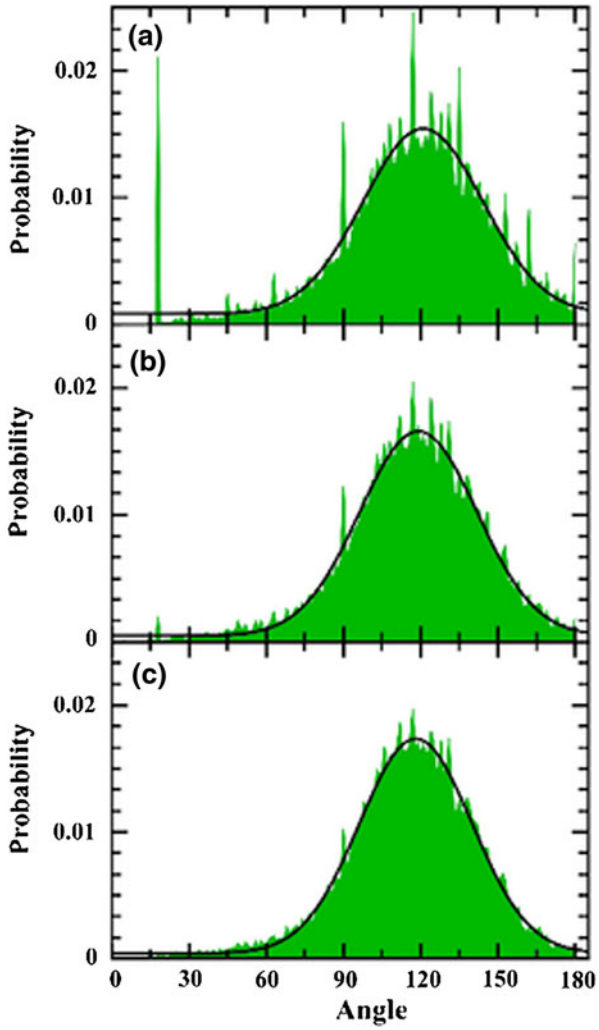

Fig. 8—Calculated angle distribution as in Fig. 6 but with minimum boundary lengths restricted to (*a*) two, (*b*) three, and (*c*) four segments. Black lines are fits to a Gaussian distribution.

Increasing the minimum to three segments results in the disappearance of the peaks at 18 deg and 162 deg, as well as all other peaks except 90 deg and 117 deg. As the "natural" lattice angle, a peak at 90 deg is to be expected for microstructures discretized on a square lattice. The peak at 117 deg is the closest square-lattice approximation to 120 deg, which is the preferred triple-junction angle for an isotropic system.

When we increase the minimum segment length to four, we observe no additional change in the angle distribution, suggesting that it is grain boundaries shorter than three segments that cause the spurious peaks in the angle distribution. In all cases, the distributions are well fit by Gaussian distributions with peaks centered close to 120 deg and χ^2 on the order of 10^{-3}.

C. *Distribution Broadening*

Harker and Parker[3] considered the distribution of angles that would be measured for a perfectly stable

grain distribution with 120 deg triple-junction angles but considering that the plane of measurement would intersect a given triple junction at an arbitrary angle. The distribution from such an analysis is, as expected, a Gaussian distribution with a peak at 120 deg but with a narrower width than our measurement gives. Harker and Parker suggest three reasons for deviations between their calculations and any measured distribution of dihedral angles, the most applicable of which is that "the interfacial angles in the specimen are not all 120 degrees," which they suggest will lead to a "spreading in the distribution function."[3] This behavior is exactly what we observe in our measurements. In fact, we expect variation in the true, 3D triple-junction angles in our microstructures for the following reasons: (1) Geometric mapping—it is impossible to map exactly a 120 deg angle onto a cubic lattice; the configuration of the grain junction will depend on its orientation with respect to the underlying lattice and will encompass a variety of mappings, each with slightly different angles. Because the spread about each "true" junction angle will be only a few degrees, the overall effect on the distribution of junction angles should be small. (2) Boundary anisotropy—the algorithm used to generate the microstructures is well known to exhibit anisotropy because of lattice effects,[17] resulting in a tendency for grain boundaries to lie along low-index directions of the lattice. This effect "pulls" boundaries away from their preferred 120 deg angle. In both simulated and real polycrystalline microstructures, the effect of grain boundary energy anisotropy may be substantial. In the structures studied here, boundary anisotropy causes our 3D triple-junction angles to deviate significantly from 120 deg; thus, the broad spread in our measured grain junction angle distribution is consistent with the predictions of Harker and Parker. Smith[10] observed a similar effect in alpha brass in which the measured triple-junction angle distribution was wider than predicted by Harker and Parker because of boundary anisotropy.

It is interesting to consider whether these distribution broadening effects can be mitigated statistically. One way to improve the statistics is to increase the number of angles measured. Although sampling more junction angles improves the distribution quality, it does not change the shape of the distribution. We also can enhance resolution by refining the microstructural mapping via increasing the number of pixels/voxels in the microstructure. The changes in the angle distribution that occur when short boundaries (which are essentially poorly refined boundaries) are removed indicate that a minimum discretization is required to resolve angles accurately. However, once the shortest boundaries are removed, we see no further change in the angle distribution, suggesting that additional refinement of the discretization does not change the results.

D. *Effects of Dimensionality*

The grain junction angle distribution for an ideal, isotropic, 2D polycrystal would be a delta function at 120 deg. Figure 9 shows the grain junction angle distribution for a 2D polycrystal evolved using the same

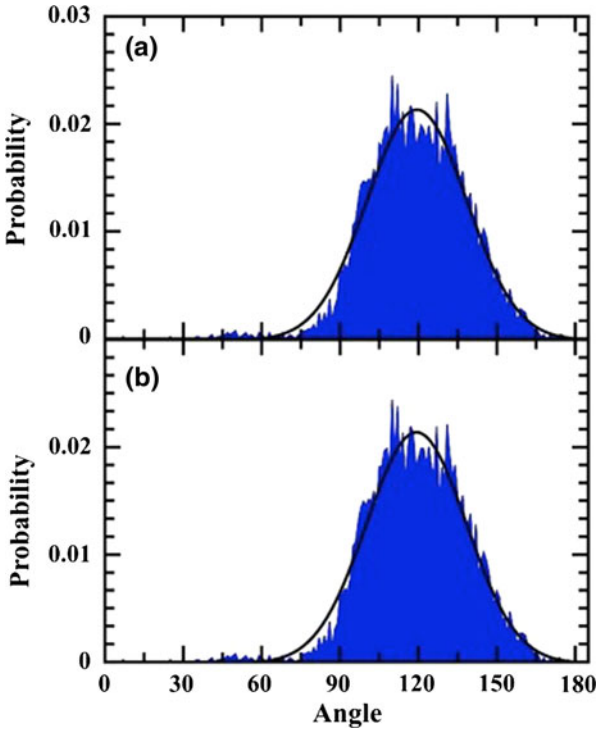

Fig. 9—Grain junction angle distribution for a 2D grain growth simulation on a 1000 × 1000 pixel square lattice with (*a*) all boundary lengths included and (*b*) a minimum boundary length of four segments. Note the difference in peaks when compared with Fig. 6.

MCPM grain growth simulation and grown under the same conditions and to the same average grain size R as the 3D system on a 1000 × 1000 square lattice with periodic boundary conditions. The grain junction angle distribution has a finite width, with angles varying from 120 deg because of factors described earlier. Smith[10] observed a similar distribution about 120 deg in experimental measurements of triple-junction angles in columnar alpha brass, which he attributed to grain boundary energy anisotropy. Smith also found that the triple-junction angle distribution was narrower in the columnar (2D) alpha brass than in equiaxed (3D) alpha brass. This finding is consistent with our observations that the 2D grain junction angle distribution (Figure 9) is narrower than the 3D distribution (Figure 6) in simulated microstructures.

Because sectioning skews apparent grain size, we expect more short boundaries in a cross section of a 3D equiaxed polycrystal than in a 2D columnar microstructure in which small grains are limited to those in the actual grain size distribution. Because it is the short boundaries that cause the anomalous peaks in the grain angle distribution (*e.g.*, Figure 6), these peaks should be minimized in a true 2D microstructure. In Figure 9, the anomalous peaks observed at low angles are absent from the distribution, implying that these peaks have their origin in the dimensionality of the simulations. To confirm this, we performed a suite of simulations on polycrystalline films in which we varied film thickness at constant grain size. When film thickness was less than average grain size, the films were perfectly columnar,

and the angle distribution matches Figure 9. Films thicker than the average grain size had equiaxed grains, and the angle distribution for the surface section matches Figure 6, including anomalous peaks. Thus, the low-angle anomalous peaks in the grain junction angle distribution are a marker for microstructural dimensionality. They provide a diagnostic to determine from a micrograph of the surface whether a microstructure is equiaxed or columnar.

E. *Validating Simulation Parameters*

The grain junction angle distribution is characteristic of a given microstructure. As such, it can be used as a metric to characterize or validate simulated or constructed microstructures. For example, the grain junction angle distribution can help determine an appropriate simulation temperature for MCPM grain growth simulations.[17] Figure 10 shows a series of MCPM simulations of identical systems run for the same Monte Carlo time with the temperature varied from $T = 0$ in which the system has a strong tendency to facet along low-index lattice planes to $T = 1.5$, which is well above the boundary roughening temperature. At $T = 0$, shown in Figure 10(a), the angle distribution is dominated by peaks at 90 deg and 180 deg, consistent with lattice faceting. As the temperature is increased to $T = 0.75$, as shown in Figure 10(b), the peaks diminish as the boundaries begin to roughen. At $T = 1.5$, shown in Figure 10(c), the boundaries are fully rough; the distribution does not vary as temperature increases further. (Note that Figure 10(c) is identical to Figure 6 and is shown here to facilitate comparisons across temperatures.) In Figures 10(d) through (f), we show the same distributions as in Figure 10(a) through (c) but with the minimum boundary length restricted to four segments to distinguish the effects of roughening from those of short segments. When the simulation temperature is too low, as in Figures 10(e) and (f), the lattice faceting peak at 90 deg remains evident, even when short segments are removed. At a sufficiently high temperature, as in Figure 10(f), the 90 deg peak disappears. Thus, absence of the 90 deg peak in the grain junction angle distribution verifies that the simulation temperature is adequate to overcome lattice faceting in MCPM simulations.

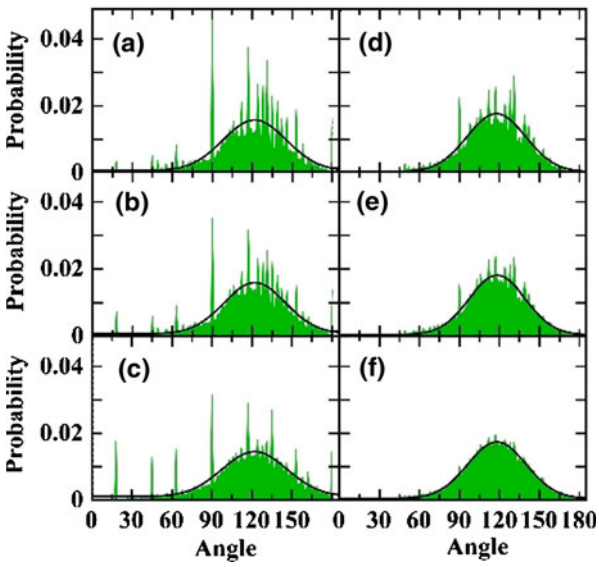

Fig. 10—Angular distribution for 3D simulations described in the text, run at simulations temperature (*a*) $T = 0$, (*b*) $T = 0.75$, and (*c*) $T = 1.5$. (*d*), (*e*), and (*f*) are the same as (*a*), (*b*), and (*c*), respectively, with the minimum boundary lengths restricted to four segments. Black lines are fits to Gaussian distributions.

F. *Characterizing Experimental Microstructures*

Analysis of grain junction angles is useful for the characterization and understanding of experimental microstructures, particularly those that are inherently discretized, such as EBSD micrographs. In Figure 11, we show calculated grain junction angle distributions for two EBSD micrographs. Figure 11(a) shows the distribution for a fully columnar Al film with 1.7 μm grains after being annealed at 450 °C for 300 minutes[13]; the microstructure is similar to that shown in Figure 1(a). The grain junction angle distribution is fit well by a Gaussian around 120 deg and has a finite width presumably from boundary anisotropy. The Al film distribution has a larger width than that observed in the simulated 2D microstructure (Figure 9) and in columnar alpha brass,[10] suggesting that grain junction distribution width depends on material system as well as dimensionality. Although the distribution has a distinct peak at 90 deg because of discretization on the square lattice, it shows no peaks at small angles.

In contrast, the distribution shown in Figure 11(b) is from EBSD data for a 1.6-mm Ni tensile bar with fully equiaxed 33-μm grains.[13] These data have undergone postanalysis to remove twins to simplify the calculation of the angular distribution. Although this distribution also is fit well by a Gaussian, the major difference between it and the distribution for the columnar structure is the low-angle peak, indicating that the prediction made previously holds true for experimental films as well; low-angle peaks are evident in 3D microstructures only and are absent in 2D films. Thus,

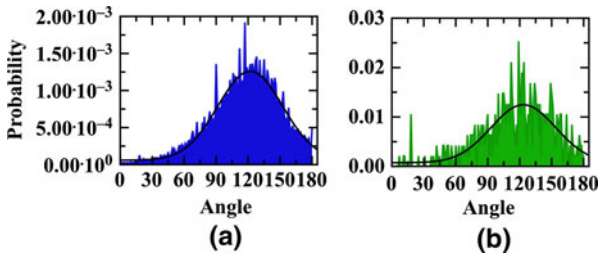

Fig. 11—Grain junction angle distribution from experimental micrographs of (*a*) columnar Al film with an average grain size of 1.7 μm and (*b*) equiaxed Ni polycrystal with 33 μm average grain size after postanalysis to remove twins. Note that the distribution in (a) is similar to the 2D distribution in Fig. 9, whereas that in (b) has the low-angle peak characteristic of the 3D distribution in Fig. 6.

grain junction angle analysis is a nondestructive test for distinguishing between columnar and equiaxed films.

IV. CONCLUSIONS

Although grain junction angles control microstructural morphology and evolution, they rarely are measured. We have developed a method, based on the optimization of the Pearson's correlation coefficient, to measure grain junction angles in planar discretized microstructures without converting or remeshing the original data. Our applications of this method to various experimental and computed microstructures suggest the following conclusions:

1. The grain junction angle distribution of equiaxed, relatively isotropic, 3D microstructures is a Gaussian distribution centered about 120 deg, as predicted by Harker and Parker.[3] The width of the distribution is larger than predicted primarily because of boundary anisotropy.
2. Short boundary segments, which occur primarily in sections of 3D microstructures, cause anomalous peaks in the grain junction angle distribution. These peaks disappear when short boundary segments are ignored in the analysis.
3. The grain junction angle distribution of true 2D (columnar) microstructures is narrower than that for 3D cross sections and lacks the anomalous peaks caused by short boundary segments.
4. The grain junction angle distribution can be used as a diagnostic to test parameters in grain growth simulations.
5. The grain junction angle distribution is a characterization metric for digitized experimental microstructures, revealing the effects of grain boundary energy anisotropy and dimensionality. Overall, the grain junction angle distribution provides a useful tool for characterizing, comparing, and understanding digitized microstructures obtained from simulation and experiment.

ACKNOWLEDGMENTS

Sandia is a multiprogram laboratory operated by Sandia Corporation, a wholly owned subsidiary of Lockheed Martin, for the U.S. Department of Energy's National Nuclear Security Administration under contract DE-AC0494AL85000. This work was supported by Sandia's Laboratory Directed Research and Development program and by the U.S. Department of Energy, Office of Basic Energy Sciences core program.

REFERENCES

1. C.S. Smith: *Grain Shapes and Other Metallurgical Applications of Topology*, ASM, Cleveland, OH, 1952.
2. C. Herring: *The Use of Classical Macroscopic Concepts in Surface Energy Problems*, University of Chicago Press, Chicago, IL, 1952.
3. D. Harker and E.R. Parker: *Trans. AIME*, 1945, vol. 34, pp. 156–201.
4. B.L. Adams, S. Ta'asan, D. Kinderlehrer, I. Livshits, D.E. Mason, C.-T. Wu, W.W. Mullins, G.S. Rohrer, A.D. Rollett, and D.M. Saylor: *Interface Sci.*, 1999, vol. 7, pp. 321–38.
5. S. Chhabra, P. Chhillar, and S. Sangal: *Prakt. Metallogr-Pr M.*, 2003, vol. 40, pp. 85–97.
6. S. Chhabra, S. Sangal, and M.N. Mungole: *J. Microsc.*, 2004, vol. 215, pp. 62–66.
7. H. Hu and C.S. Smith: *Acta Metall. Mater.*, 1956, vol. 4, pp. 638–46.
8. D.M. Saylor, A. Morawiec, and G.S. Rohrer: *Acta Mater.*, 2003, vol. 51, pp. 3675–86.
9. D.M. Saylor, A. Morawiec, and G.S. Rohrer: *Acta Mater.*, 2003, vol. 51, pp. 3663–74.
10. C.S. Smith: *Trans. AIME*, 1948, vol. 175, pp. 15–51.
11. V. Thaveeprungsriporn, P. Sinsrok, and D. Thong-Aram: *Scripta Mater.*, 2001, vol. 44, pp. 67–71.
12. S.M. Mahadevan and D. Casasent: *Ultramicroscopy*, 2003, vol. 96, pp. 153–62.
13. G.S. Rohrer: Personal communication, June 23, 2009.
14. J.L. Rodgers and W.A. Nicewander: *Amer. Stat.*, 1988, vol. 42, pp. 59–66.
15. M. Anderson, G. Grest, and D. Srolovitz: *Phil. Mag. B*, 1989, vol. 59, pp. 293–329.
16. M. Anderson, D. Srolovitz, G. Grest, and P. Sahni: *Acta Metall. Mater.*, 1984, vol. 32, pp. 783–91.
17. E. Holm, J.A. Glazier, D. Srolovitz, and G. Grest: *Phys. Rev. A*, 1991, vol. 43, pp. 2662–68.